JOURNAL OF PROPULSION AND POWER
Vol. 26, No. 5, September–October 2010

Molecular Weight and Shock-Wave Effects on Transverse Injection in Supersonic Flow

Joseph A. Schetz,* Luca Maddalena,† and Scott K. Burger‡
Virginia Polytechnic Institute and State University, Blacksburg, Virginia 24061

DOI: 10.2514/1.49355

An experimental study of the effects of injectant molecular weight on transverse-jet mixing in a supersonic crossflow is reported. In addition, the effects of an oblique shock impinging near the injection station were investigated. The examined gaseous injector is circular in geometry and angled downstream at 30 deg to the horizontal. Test conditions involved sonic injection of helium, methane, and air at a jet-to-freestream momentum flux ratio of 2.1 into a nominal Mach 4 air cross stream with average Reynolds number 5.77e + 7 per meter to provide a range of injectant molecular weights from 4–29. Sampling probe measurements were used to determine the local helium and methane concentration. A miniature five-hole pressure probe, pitot and cone-static pressure probes, and a diffuser-thermocouple probe were employed to document the flow. The goals of this effort are twofold. The first goal is to broaden and enrich the database for transverse injection in high-speed flows. Second, these data will aid greatly in the development of advanced turbulence models with a wide range of applicability for high-speed mixing flows. The main experimental results showed that an impinging shock reduces penetration and increases mixing for injectants of all molecular weights. Higher molecular weight injectant seems to increase penetration, but the effect is weak. The effects of shock impingement were strongest when this occurred downstream of, and closest to, the injection port.

Nomenclature

A_j	=	injector area
C_d	=	discharge coefficient
$C_{p\eta}$, C_{pz}	=	angular pressure coefficients
d_j	=	jet diameter
d_{eff}	=	effective diameter
f	=	stoichiometric fuel-air ratio
M	=	Mach number
$M_{x,y,z}$	=	Mach number components
$\dot{m}$	=	mass flow rate
PA	=	average pressure on five-hole probe
$P1, 2, 3, 4, 5$	=	pressures on five-hole probe
p	=	(static) pressure
$p_{t,\text{Pitot}}$	=	pitot pressure
q	=	dynamic pressure
$\bar{q}$	=	jet-to-freestream momentum flux ratio
$\mathbb{R}$	=	universal gas constant
T	=	temperature
u	=	flow velocity
$\mathbb{V}_y(d_{\text{eff}})$	=	vortex center height
$\mathbb{V}_z(d_{\text{eff}})$	=	horizontal center vortex spacing
W	=	injectant molecular weight
X	=	axial distance downstream of injector center
Y	=	lateral distance from the injector centerline
$y^{\pm}$	=	plume width
Z	=	vertical distance from the wall
$z_{\alpha,\max}$	=	plume core height
α	=	mass fraction
γ	=	ratio of specific heats
θ	=	pitch angle
ρ	=	density
φ	=	roll angle

Subscripts

j	=	jet-exit property
t	=	total condition
∞	=	freestream property

Presented as Paper 2009-7315 at the Spaceplanes and Hypersonics Conference, Bremen, Germany, 19–22 October 2009; received 13 February 2010; revision received 23 May 2010; accepted for publication 1 June 2010.

*Fred D. Durham Chair, Department of Aerospace and Ocean Engineering, 215 Randolph Hall. Life Fellow AIAA.

†Graduate Research Assistant; currently Assistant Professor, University of Texas at Arlington, Arlington, TX. Member AIAA.

‡Graduate Research Assistant, Department of Aerospace and Ocean Engineering, 215 Randolph Hall. Member AIAA.

I. Introduction

AIR-BREATHING hypersonic flight vehicles, such as the supersonic combustion ramjet (scramjet) are characterized by extremely small flow residence times in the engine. This short residence time of the flow particularly handicaps the fuel/air mixing process, which needs to be enhanced significantly if the fuel is to be effectively mixed with the incoming air. To design injection systems with enhanced penetration and mixing, current levels of understanding and prediction capabilities must first be significantly improved. Also, the applicability of the turbulence models in current computational fluid dynamics codes must be expanded, and the level of uncertainty in the predictions must be lowered. One area that has been identified as needing further study is the influence of injectant molecular weight. Another subject of particular interest for understanding mixing enhancement at hyper-velocities is shock-enhancement mixing behavior, in which the interaction between the mixing layer and an oblique shock creates strong axial vortices that stretch the fuel/air interface. The interaction of a mixing layer composed of a light gas accelerating in a heavy gas with an oblique shock wave induces a misalignment between the density gradient in the mixing layer and the pressure gradient of the shock wave. This misalignment creates instability in the fluid interface and then enhanced turbulent mixing. In addition, shocks are a ubiquitous feature in supersonic combustion engines, so understanding their influence on mixing is a critical need.

A large number of experiments have been performed in the field of injection in supersonic flow using numerous techniques. A representative sample of previous works is listed here as [1–18]. Extensive reviews of injector mixing characteristics are given in [19–22].

The first aim of the present work is to examine the effects of injectant molecular weight variations on transverse-jet mixing in a Mach 4 crossflow. The injectants considered here are helium ($W = 4.00$), methane ($W = 16.04$) and air ($W = 28.97$). Second, since shocks are so common in scramjet combustors, their influence on penetration and mixing was also studied by arranging for an oblique shock to impinge near the injection station. One can also anticipate an important influence of molecular weight here because of the importance of density gradients on the generation of vorticity by baroclinic torque.

A shock passage through the density gradient in mixing gases of different densities provides a pressure gradient and deposits a distribution of vorticity. The nonalignment of the density and the pressure gradients creates vorticity through baroclinic torque, and the amount of generated vorticity will vary as the baroclinic torque term varies [23]. The baroclinic torque term in the vorticity equation, the third term on the right hand side of Eq. (1), represents the production of vorticity in compressible flows:

$$\frac{\mathrm{D}(\omega)}{\mathrm{D}t} = -\boldsymbol{\omega}(\nabla \cdot \mathbf{V}) + (\boldsymbol{\omega} \cdot \nabla \mathbf{V}) + \frac{1}{\rho^2}(\nabla\rho \times \nabla p) + \nu\nabla\boldsymbol{\omega} \quad (1)$$

The cross product is nonzero when the gradients are nonparallel. Therefore, to generate vorticity the pressure and the density must have significant variations that are not parallel with each other; the largest misalignment and the largest gradients will create the largest change in vorticity. If a shock is imposed on a density gradient, the pressure gradient across the shock cause torques in the fluid. These torques cause the fluid elements to rotate and change vorticity, thus influencing the subsequent vortex dynamics. The understanding of the relative magnitude of the terms described above is provided by the nondimensional form of Eq. (1). As shown by the work in [24], in supersonic flows the dilatational term, $-\omega(\nabla \cdot \mathbf{V})$, is of the same order of magnitude as the vortex stretching, $\omega \cdot \nabla\mathbf{V}$, and the baroclinic term $(\nabla\rho \times \nabla p)/\rho^2$. This analysis establishes that for the flows under consideration the rate of change of vorticity in a Lagrangian frame of reference is not exclusively driven by vortex stretching (as for subsonic flows) but also by dilatational and baroclinic effects.

There have been some previous studies of some aspects of injectant molecular weight effects and shock impingement effects in the literature (see References for examples), but there has not been a comprehensive study of the combined effects. That is the main purpose of the present study.

A pictorial description of the problem studied here is given in Fig. 1. For three different runs, a single oblique shock was impinged upon an injected light gas stream at different downstream locations corresponding to shock surface impact locations of about 2, 8 and 16 effective jet diameters downstream of the injector center, if the oblique shock is projected straight from its direction in the freestream to the wall. Some tests were also run with the shock impinging upstream of the injector.

II. Experimental Methods

A. Facilities

Experiments were performed in the Virginia Polytechnic Institute and State University (Virginia Tech) supersonic wind tunnel with a Mach 4 nozzle. This is a blow-down type tunnel with a 23 × 23 cm test section and a maximum run time of approximately 25 s. The tunnel is charged by an Ingersoll–Rand, type 4-HHE-4, water cooled, four stage compressor equipped with a dryer and separator to remove water vapor and oil during operation. Compressed air is stored in two tanks with a combined volume of 23 m^3. During runs, these tanks feed into a plenum through a pneumatic butterfly valve which is controlled by a PID program in order to maintain a constant pressure. The pressure typically varied by less than ±35 kPa from its set point of 1034 kPa during the initial oscillations, settling within 1% of the desired value. The total temperature was approximately 300 K.

The injector and sampling station were installed in the floor of the test section as shown in Fig. 2. A circular, single-port, flush wall injector was used for these experiments. The injector had a diameter, $d_j = 3.23$ mm, and was inclined at an angle of 30 deg to the wall. Dimensions were normalized to the effective diameter:

$$d_{\text{eff}} = \sqrt{C_d}\, d_j \quad (2)$$

where the discharge coefficient $C_d = 0.88$, giving $d_{\text{eff}} = 3.03$ mm. A diagram of the injector insert is shown in Fig. 3.

The boundary layer thickness at the measurement station has been investigated in order to characterize the freestream conditions, and it

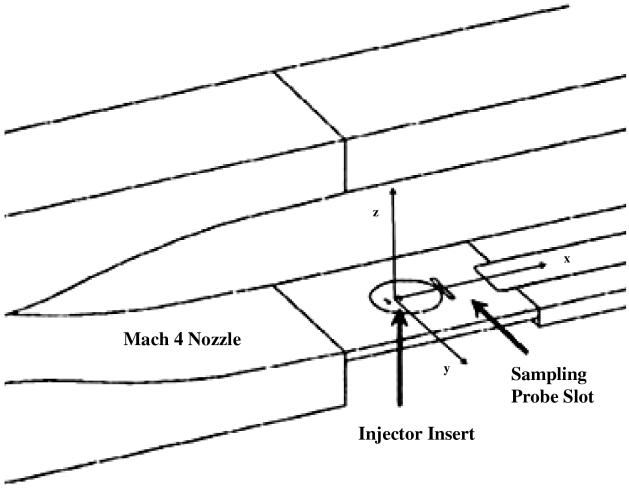

Fig. 2 Experimental setup.

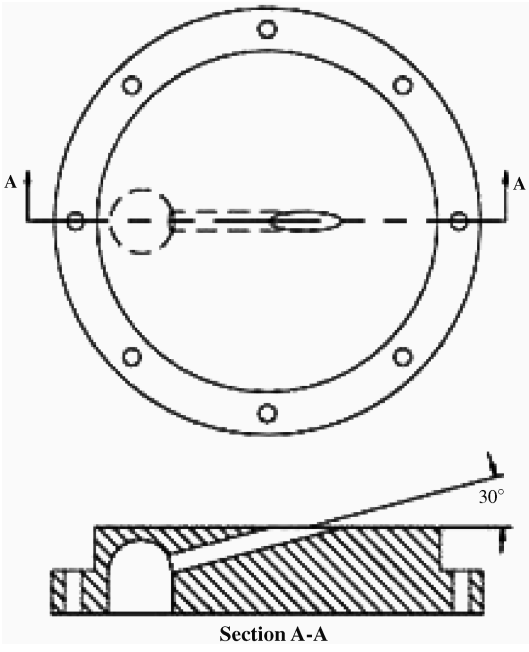

Fig. 3 Single circular hole injector insert, diameter 3.23 mm, flow left to right.

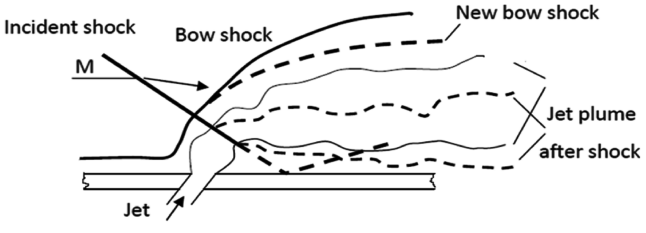

Fig. 1 Schematic of the shock/transverse-jet interaction setup.

has been found to be approximately 20 mm. This survey was performed using the five-hole probe and traverse system described later. Thus, the boundary layer thickness is substantially greater than the injector diameter. That is representative of the conditions expected in scramjet engines where the air stream has traversed a long distance along the inlet before reaching the injectors in the combustor. There have been few systematic studies of boundary layer thickness effects on jet injection flows. [25] contains such a study, but the emphasis was on jet interaction flows for vehicle control applications.

For the shock interaction studies, a two-dimensional shock generator was used to create an oblique shock of 18.3 ± 0.5 deg, generating a pressure ratio of $1.67 \pm .05$, to impinge upon the injection jet. The shock generator consists of a wedge creating a turning angle of 5.3 deg and a 20 cm wide leading edge attached to a sting mount as shown in Fig. 4. Shadowgraphs of the region studied near the jet in Fig. 5 show that no extraneous disturbances were introduced into the flow in addition to the desired oblique shock.

B. Injection Characteristics

Injection was sonic for all injectants. To compare the results for injection of differing gases, the jet to freestream dynamic pressure ratio, defined below, was held constant at 2.1 for all injectants:

$$\bar{q} = \frac{(\rho u^2)_j}{(\rho u^2)_\infty} = \frac{(p\gamma M^2)_j}{(p\gamma M^2)_\infty} \tag{3}$$

To hold the dynamic pressure ratio constant, the injection mass flow, $\dot{m}_j$, was varied:

$$\dot{m}_j = \rho_j u_j A_j \tag{4}$$

The mass flows resulting in $\bar{q} = 2.1$ are as follows: for air (295 K) $\dot{m}_j = 10.0$ g/s for methane (295 K), $\dot{m}_j = 6.7$ g/s and for heated helium (313 K) $\dot{m}_j = 3.4$ g/s. Mass flow rate was calculated by measuring the pressure drop across an orifice flow plate, and was maintained to within $\pm 5\%$ of the nominal value during all runs.

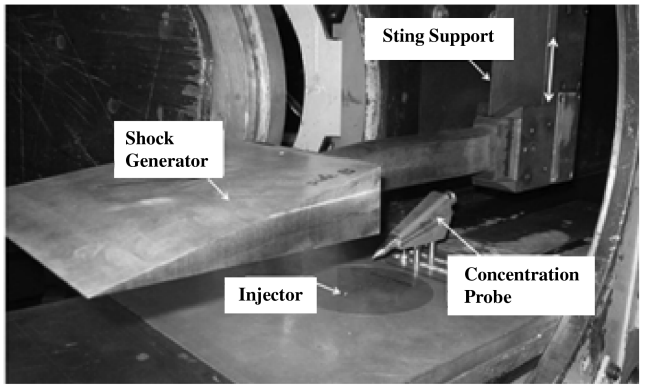

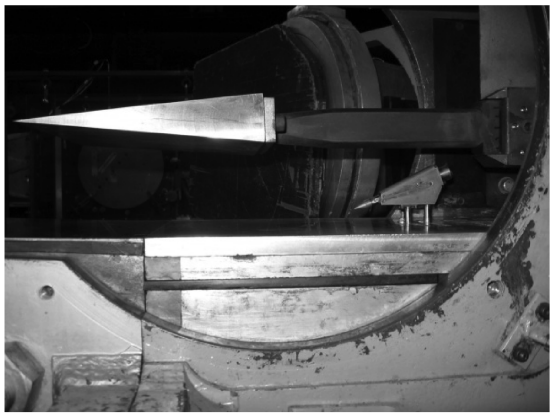

Fig. 4 Shock generator in test configuration.

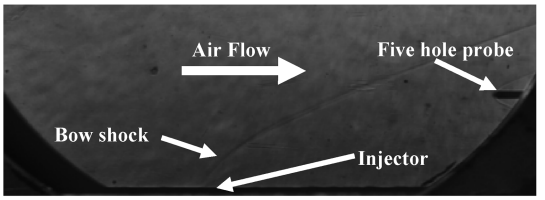

a) Air injection without an impinging shock

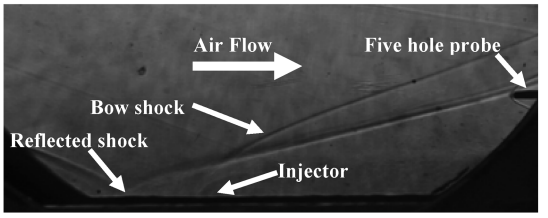

b) Air injection with shock reflection 4.5 effective diameters upstream of the injector

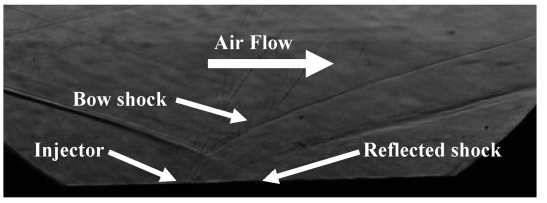

c) Air injection with shock reflection 2.5 effective diameters downstream of the injector

Fig. 5 Shadowgraphs of the flow near the injector without and with impinging shocks.

C. Probe Traverse and Data Acquisition

Data were taken by means of probes mounted on a two-axis traverse system. The traverse speed was 5 mm/s, which allowed an entire vertical section of data to be taken in each run with 200 ms stops at each vertical station, so that at least 50 samples could be averaged to produce the data at each point. Between runs, the traverse was moved laterally to the next horizontal station. Data were recorded on a PC with a 16-channel, 16-bit analog-to-digital converter and a 64-channel multiplexer, both with a built-in cold-junction compensator for temperature measurements. Data were taken at 500 Hz. The probe position was controlled by a LabView program integrated into the tunnel control program.

D. Concentration Probe

The first probe used was a gas species concentration probe developed by Dr. Ng and his associates at Virginia Tech [26]. A diagram of the probe is shown in Fig. 6. The diameter of both the sampling plane and the choked orifice was 0.63 mm. The flow channel expands to a diameter of 3.8 mm so that a normal shock is formed in front of the sensors. Mechanical aspiration by means of a vacuum pump ensures that the orifice remains choked, so that a stream tube equal in area to the probe tip enters undisturbed. The diverging internal flow section creates a very low velocity in the region of the sensors, so that conditions can be treated as stagnation

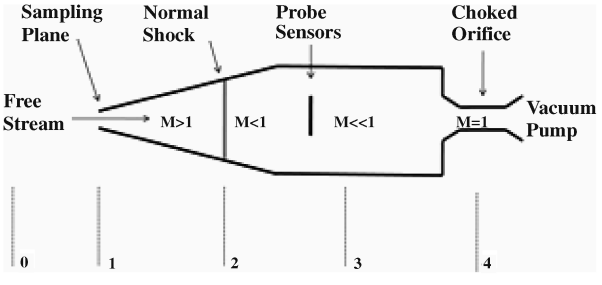

Fig. 6 Diagram of the concentration probe.

conditions. The probe used three measurements taken within its housing to determine the molar fraction of a binary mixture of gases. Temperature was measured with a *K*-type thermocouple, and pressure was measured with an externally mounted pressure transducer connected to an internal port. Additionally, voltage was recorded from a platinum hot-film sensor using a constant-temperature anemometer and a CTA bridge. This probe design allows only measurements of the mean concentration. The frequency response of the probe is limited by the response of the pressure measurement and the flush-out time of the probe, which is the time required for a fluid particle to travel from the sensor plane to the choked orifice [26]. During the measurements, the probe was maintained at a given location for 200 ms which was determined to insure a steady measurement.

The probe was calibrated by connecting it to a tank with the desired gas mixture in known concentrations at varying pressure. The tank was first pumped to a vacuum and then filled with controlled partial pressures of the desired species. The tank was initially pressurized to 276 kPa with this known mixture, and then emptied slowly with the aid of the vacuum pump so that the calibration would cover the necessary range of pressures. An example set of calibration data is shown in Fig. 7 for a mixture of methane and air. The probe operates by using variations in the gas constant, i.e., mixture molecular weight, so it is less sensitive for methane in air mixtures than for helium in air mixtures. By careful calibration, the uncertainty was maintained at ± 0.01 for helium or methane mass fraction.

E. Aerothermodynamic Probing

Aerothermodynamic probing was accomplished by means of pitot, cone-static and total temperature probes. The pitot probe had an outer diameter of 1.59 mm and an inner diameter of 1.04 mm, which gave a capture area of 0.85 mm^2. The cone-static probe consisted of a cone with a 10 deg half-angle and an outer diameter of 1.59 mm. There were four small ports arranged around the cone to reduce misalignment effects of the probe with respect to the flow. The uncertainty in pressure measurement was evaluated to be ± 0.06 atm.

Total temperature was measured with a rake consisting of three tubes of 1.59 mm outer diameter spaced 6.4 mm apart. Each tube had an inner diameter of 1.04 mm giving a capture area of 0.85 mm^2. The total temperature probes also had 4 small ports to improve the recovery factor. The ratio of capture to recovery area was 5 to 1 resulting in a probe recovery factor 0.97. Exposed junction type-*E* thermocouples with 0.25 mm diameter bead were placed inside the three total temperature probes. The uncertainty on temperature measurement was evaluated to be ± 2 K.

F. Five-Hole Pressure Probe

The final probe used in this study was a customized five-hole probe manufactured by Aeroprobe, Inc. The conical tip is 1.65 mm in diameter with a pressure port at the tip and four more arrayed around the cone surface. The pressure ports have an inner diameter of 0.419 mm and each contains a miniature piezoresistive transducer. The semivertex angle is 45 deg. Having imbedded transducers allows for a 99% step response time of only 11 ms. Its power supply output is ± 13.5 VDC which is filtered through a two-stage active filter and regulated to 10 V for sensors and ± 12 V for amplifier modules. Individual amplifier gain is set for the full range of sensors to ± 5 V.

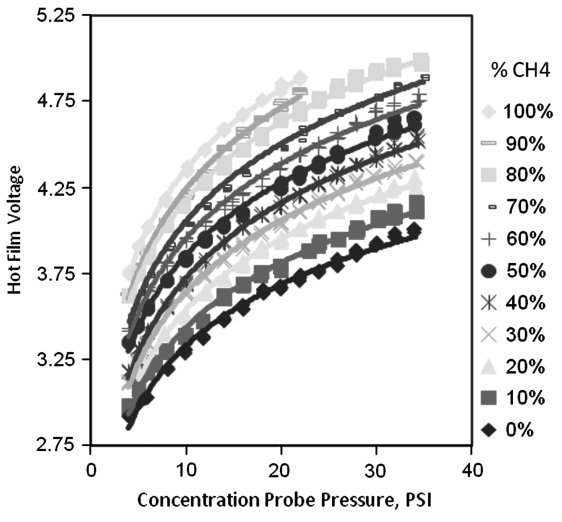

Fig. 7 Concentration probe calibration for methane in air.

Through a calibration process (based on the initial work of Centolanzi [27]), the local flow angularity and Mach number can be related to the pressure measurements of diametrically opposed pressure ports on the probe's conical surface. To determine the angularity, two coefficients are defined:

$$C_{\rho\eta} = \frac{P5 - P3}{q}, \quad C_{pz} = \frac{P4 - P2}{q} \tag{5}$$

where $P2$, $P3$, $P4$, $P5$ are the port pressures and q is the dynamic pressure. These coefficients can be uniquely related to an angle of pitch, θ, and roll, φ.

The five-hole probe was calibrated in the Mach 3.1 Supersonic Free Jet Facility at Virginia Tech which was designed for that purpose. The probe was mounted on a support that could pivot the probe in both pitch and yaw. During a period of continuous run, the probe was moved through a range of angles of ± 18 deg in both axes with measurements taken at increments of 0.9 deg up to 9 and 1.8 deg for the remainder of the range. The uncertainty in the flow angle is $\pm 0.5°$.

The angularity map can be treated as independent of Mach number. To calibrate for Mach number, the probe was traversed through the boundary layer of the Virginia Tech supersonic wind tunnel where the Mach number was measured separately using a 10 deg cone-static probe and a pitot probe mounted together. The ratio of the center port pressure to the average of outer port pressures $P1/\mathrm{PA}$ was then plotted vs Mach number, and a power curve fit was employed. Once the Mach number and the flow angularity have been determined, then the flow components can be computed as

$$M_x = -M\sin(\theta)\sin(\phi) \qquad M_y = -M\sin(\theta)\cos(\phi)$$
$$M_z = M\cos(\theta) \tag{6}$$

Since $P1/\mathrm{PA}$ is a function of flow direction, an additional iteration is performed using a correction factor map to increase the accuracy of the computed Mach number.

Because this calibration curve is for air, there is the possibility of introducing error when sampling a mixed flow of air and methane in the jet plume, where the ratio of specific heats, γ, is not identical to that of air. To analyze the sensitivity to the mixture composition (specific heats ratios), Taylor–McColl solutions were performed for the similar case of a 45 deg half-angle pointed cone. This analysis predicts the error generated by representative mixtures (one for the average plume concentration and the second one for the maximum concentration for methane injection cases as reported from the measurements in the jet's plume) with respect to the case with air only. These conditions are for specific heat ratios of $\gamma = 1.37$ and $\gamma = 1.33$, respectively. This probe was not used for helium injection.

The error in percent of nominal Mach number declines with decreasing Mach number. Since the high concentrations of methane occur inside the injection plume where Mach number is low, the error is minimized. The maximum concentrations occur where the Mach number is approximately 2.5, leading to a maximum error of 5% in Mach number.

III. Experimental Results

The concentration measurements were taken 13.9 d_{eff} downstream of the injector center, and other measurements were taken 16.4 d_{eff} downstream. The different locations were necessitated by the dimensions of the various probes and the geometry of the wind tunnel. Height above the wall and horizontal distance were selected to be sufficient to capture the flow field of the plume, approximately

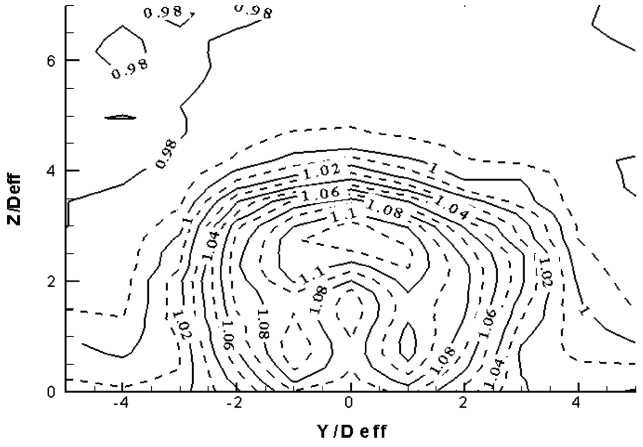

a) Shock at $X/d_{eff} = 2$

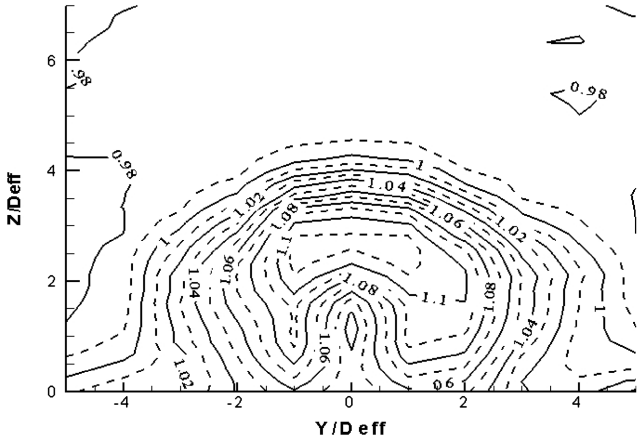

b) Shock at $X/d_{eff} = 8$

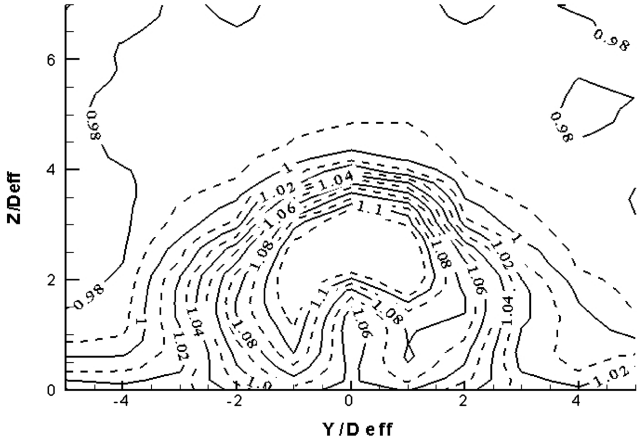

c) Shock at $X/d_{eff} = 16$

Fig. 8 Normalized total temperature contours in the (*Y*-*Z* plane) at $X/d_{\text{eff}} = 16.4$ for helium injection.

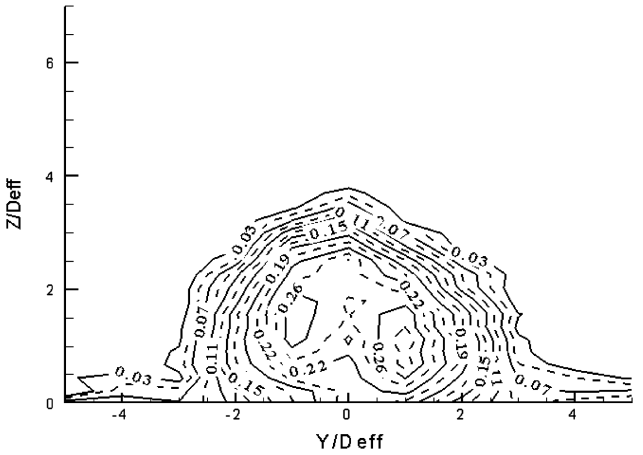

a) Shock at $X/d_{eff} = 2$

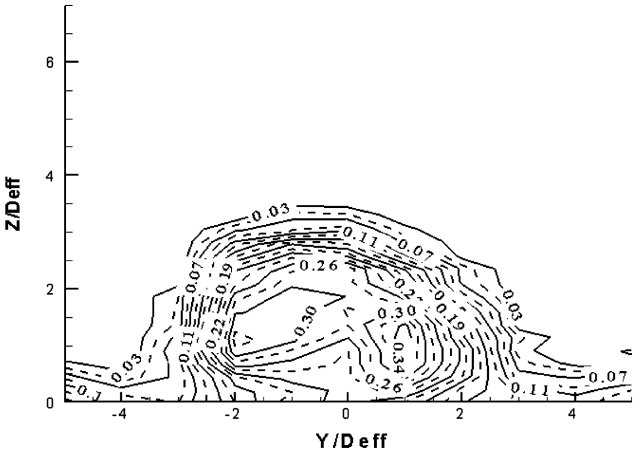

b) Shock at $X/d_{eff} = 8$

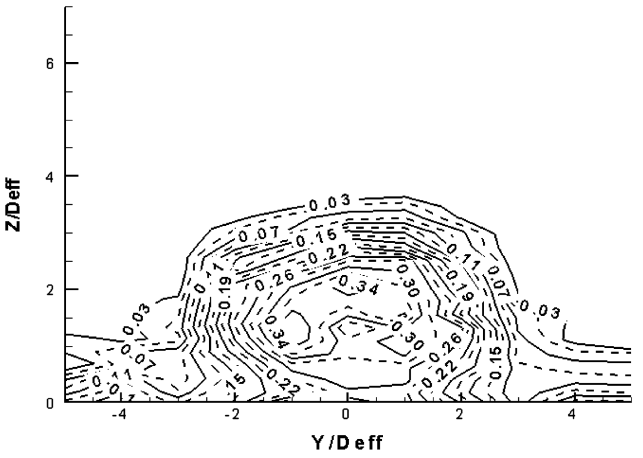

c) Shock at $X/d_{eff} = 16$

Fig. 9 Mass fraction contours in the (*Y*-*Z* plane) at $X/d_{\text{eff}} = 16.4$ for helium injection.

$Y_{\max} = \pm 4$–$5d_{\text{eff}}$ from the injector centerline and $Z_{\max} = 7$–$8d_{\text{eff}}$ above the wall. Data were taken as close to the wall as probe geometry allowed. Data shown below this level are an extrapolation based on wall assumptions. The estimated uncertainty in the grid origin location is $\pm 0.2d_{\text{eff}}$, and the estimated uncertainty of grid points relative to each other is $\pm 0.003d_{\text{eff}}$.

A. Helium Injection Cases

Results for heated (313 K) helium injection with a shock impinging at 2, 8 or 16 effective diameters downstream of the injector center are presented first. Comparable results for the same injector

Table 1 Global parameters deduced from concentration contour plots for helium injection

Parameter	$\alpha_{\max}$	$z_{\alpha,\max}/d_{\text{eff}}$	$y^{\pm}$
No-shock case [13]	0.34	2.6	6.9
Shock at $2d_{\text{eff}}$	0.3	1	5.9
Shock at $8d_{\text{eff}}$	0.35	1.2	6.5
Shock at $16d_{\text{eff}}$	0.37	1.5	6.4

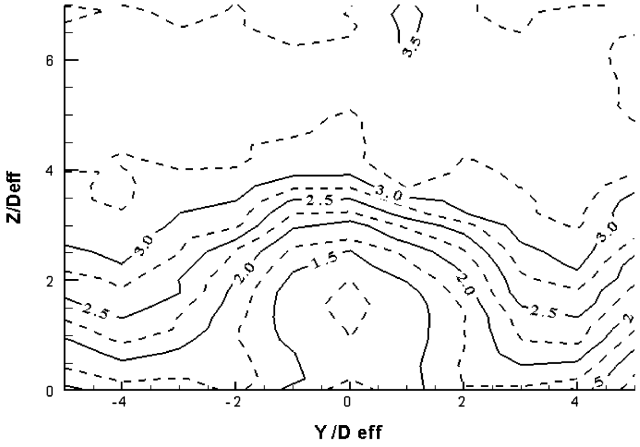

a) Shock at $X/d_{eff} = 2$

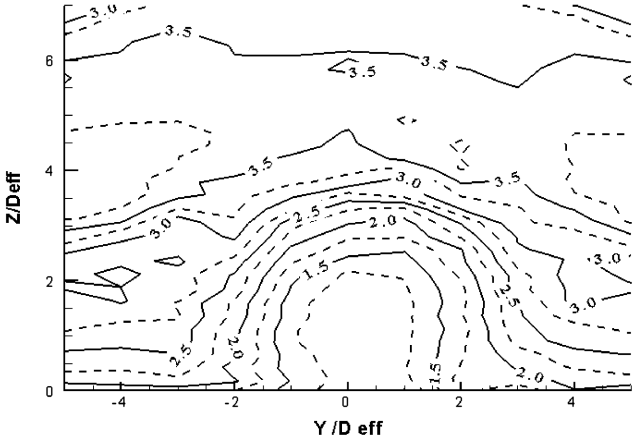

b) Shock at $X/d_{eff} = 8$

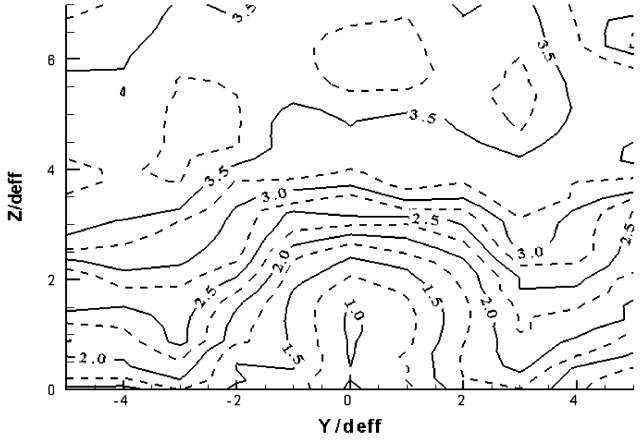

c) Shock at $X/d_{eff} = 16$

Fig. 10 Mach number contours in the (Y-Z plane) at $X/d_{\text{eff}} = 16.4$ for helium injection.

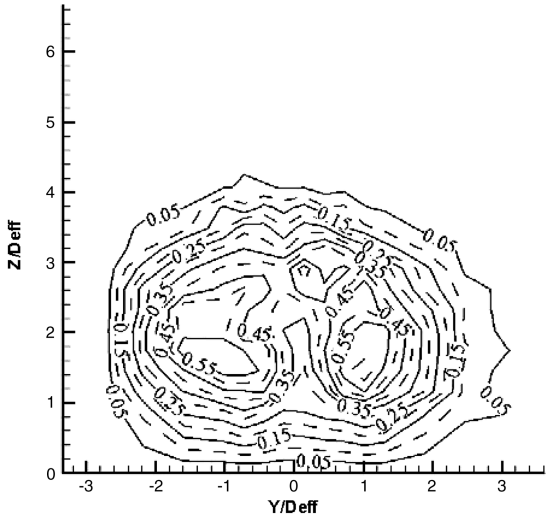

a) Undisturbed flow (No-shock case)

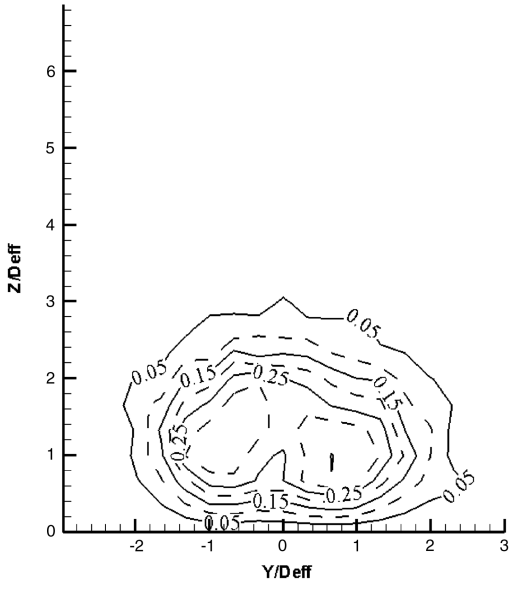

b) Shock impinging downstream of injector at $X/d_{eff} = 2.5$

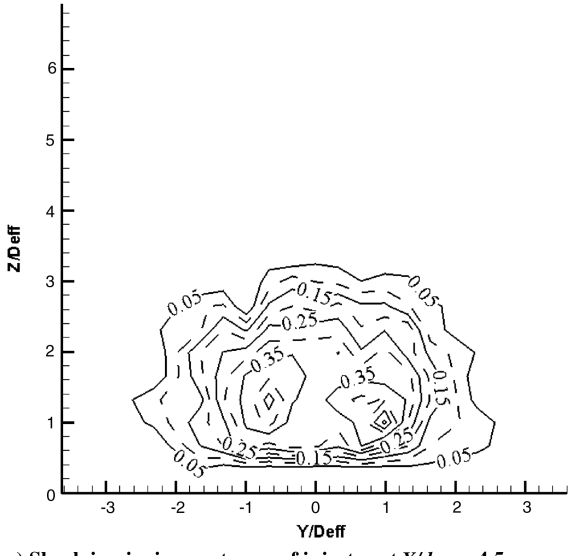

c) Shock impinging upstream of injector at $X/d_{eff} = -4.5$

Fig. 11 Mass fraction contours in the (Y-Z plane) at $X/d_{\text{eff}} = 16.4$ for methane injection.

and test conditions without shock impingement can be found in [13]. Total temperature and mass fraction contours are presented in Fig. 8 and 9. The local total temperature contours are normalized by the freestream total temperature in Fig. 8. These isothermal contours illustrate the total temperature field produced by the injection process and allow for a qualitative assessment of penetration and mixing produced in the three cases under investigation. A distinctive feature is the horseshoe-shaped structure of the plume. This shape is associated with the counter-rotating vortex pair (CVP) structure generated by the interaction of a jet in a crossflow. Next, consider the corresponding mass fraction contours in Fig. 9. Table 1 lists some

gross parameters of the results. The plume core height is quantified as the vertical location of the maximum mass fraction, $z_{\alpha,\max}/d_{\text{eff}}$. The plume width, $y^{\pm}$, is the width of concentrations above the hydrogen/air stoichiometric value of 2.92%. As shown in the plots and Table 1, shock impingement at two effective diameters downstream represents the situation that is most sensitive to the effects of the shock. In fact, the maximum concentration is lowest, for this case, at $\alpha_{\max} = 0.30$. Cases with shock impingement at 8 and 16 effective diameters downstream are almost identical in terms of maximum concentration and almost the same value as the No-shock case [13]. The trend of the total temperature contours in the plume compared with the concentration contours clearly shows that an attempt to estimate the mixing characteristics based upon temperature alone can lead to a misinterpretation of the actual physics.

The results presented in Table 1 show the no-shock case [13] having greater penetration (indicated by $z_{\alpha,\max}/d_{\text{eff}}$) than the cases with the shock. This is due to the change in flow direction caused by the shock. For all cases with shock impingement, the center of mass of the plume is nearly insensitive to the shock impingement position. The lateral spreading is slightly higher for the No-shock case than the cases with shock impingement. The maximum concentration is lowest and the mixing efficiency is highest for the with shock impingement closest to the injection station. Finally, the sampling area of the probes can be noted to be a small fraction of the plume area.

Mach number contours of the flow fields for the three shock impingement cases are shown in Fig. 10. Even in this complex, three-dimensional situation in which the planar shock impinges upon the bow shock generated by the transverse injection of helium, it is possible to recognize the edge of the jet. The sharp decrease in Mach number is caused by the mixing of low Mach number gas from the jet and the higher Mach number gas from the freestream, shock structure in the plume, viscous forces in the boundary layer, and the variation of the jet bow shock strength. The shock at $X/d_{\text{eff}} = 2$ case is subjected to both the incident and reflected shock by the measurement plane, and the Mach number is lowest compared with the other cases. Only the incident shock effect is captured in the measurement plane for the shock at $X/d_{\text{eff}} = 8$ and 16 cases.

B. Methane Injection Cases

Based on the results from the shock impingement tests with helium injection, the focus of the tests with methane and air injection was placed on shock impingement locations near the injector, one downstream and one upstream. Data are presented for three cases: 1) injection into an undisturbed freestream (no-shock case), 2) injection with the shock impinging 2.5 ± 0.2 effective diameters downstream of the injector center, and 3) injection with the shock impinging 4.5 ± 0.2 effective diameters upstream of the injector center.

Mass fraction data obtained from the concentration probe for methane injection is given in the form of contour plots in Fig. 11. The CVP is evidenced by the double plume core that is formed. The plume core height is quantified as the vertical location of the maximum mass fraction, $z_{\alpha,\max}/d_{\text{eff}}$. The plume width, $y^{\pm}$, is defined here as the width of concentrations above the methane/air stoichiometric value of 6.16%. These values are given in Table 2 below. Clearly, a shock impinging near the injection station increases mixing, whether it impinges upstream or downstream. The increase is larger for the downstream impingement. Recall that we also found enhanced mixing for shock impingement downstream of and nearby helium injection.

Table 2 Global parameters deduced from concentration contour plots for methane injection

Parameter	$\alpha_{\max}$	$z_{\alpha,\max}/d_{\text{eff}}$	$y^{\pm}$
No-shock case	0.64	1.45	4.7
Shock at $2.5d_{\text{eff}}$	0.35	0.99	4.3
Shock at $-4.5d_{\text{eff}}$	0.47	1.32	4.6

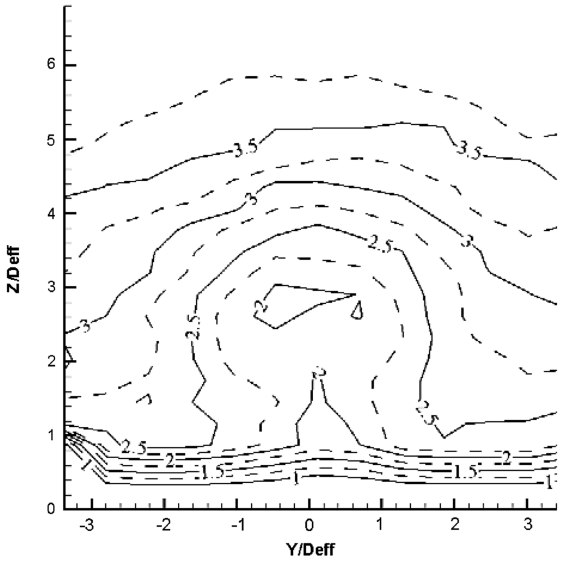

a) Undisturbed flow (No-shock case)

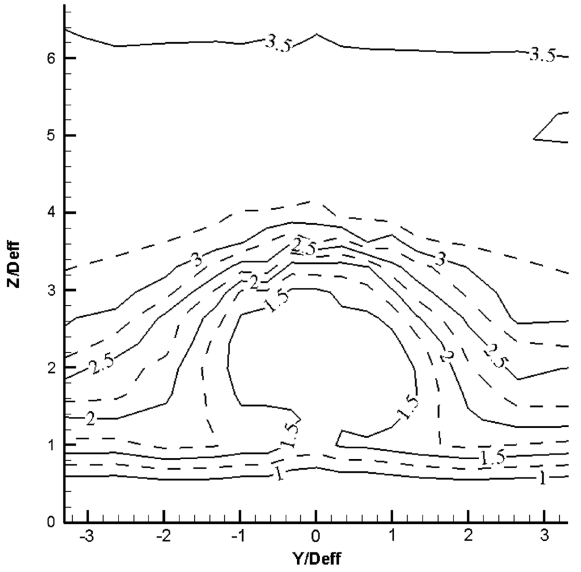

b) Shock impinging downstream of injector at $X/d_{eff} = 2.5$

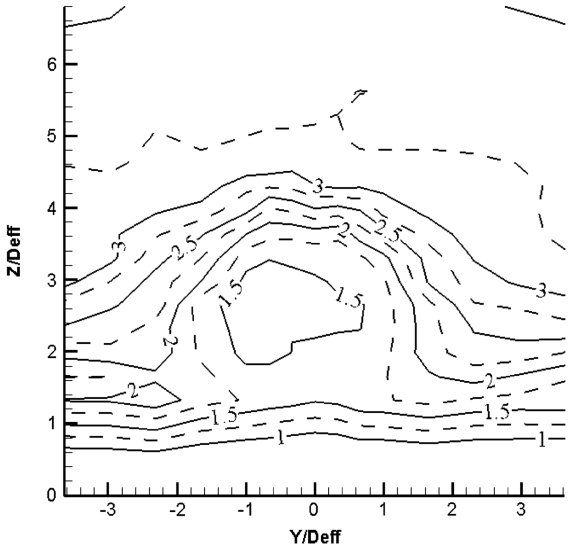

c) Shock impinging upstream of injector at $X/d_{eff} = -4.5$

Fig. 12 Streamwise Mach number contours in the (*Y*-*Z* plane) at $X/d_{\text{eff}} = 13.9$ for methane injection.

The plume core is lower for the upstream shock impingement case than for the no-shock case, indicating that the plume does not penetrate as far due to the higher pressure behind the shock. For the case of shock impingement downstream of the injector, the plume core is lower than the upstream shock impingement case, showing that the plume is influenced by the strong pressure gradient produced by the shock. The same qualitative effect of plume compression by the shock was observed with helium injection, although to a lesser degree, with less vertical compression of the plume.

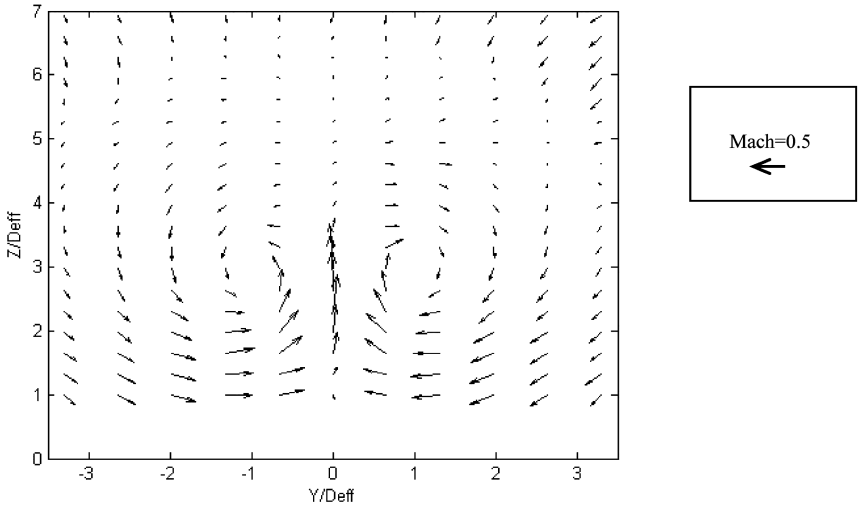

a) Undisturbed flow (No-shock case)

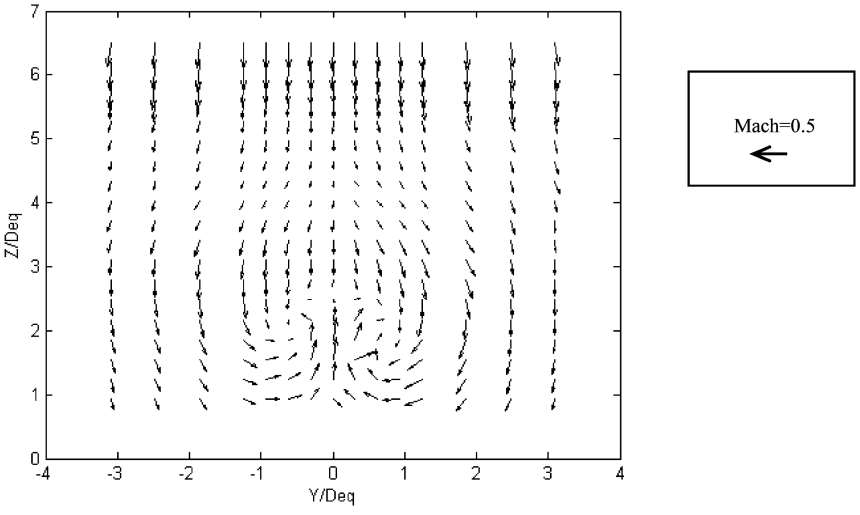

b) Shock impinging downstream of injector at $X/d_{eff} = 2.5$

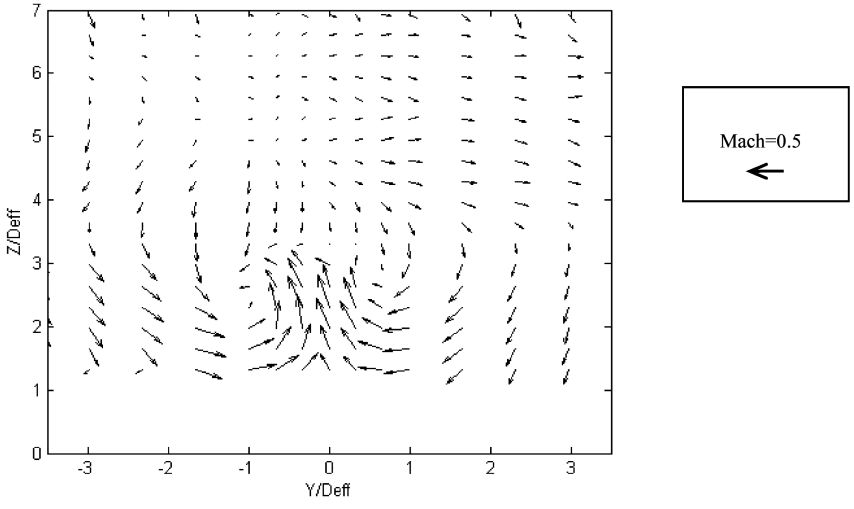

c) Shock impinging upstream of injector at $X/d_{eff} = -4.5$

Fig. 13 Transverse Mach number contours in the (Y-Z plane) at $X/d_{\mathrm{eff}} = 13.9$ for methane injection.

The streamwise Mach number data from the five-hole probe surveys for methane injection into air is presented as a series of contour plots in Figs. 12a–12c.

The region influenced by the injection plume can be seen as an area of reduced Mach number as the relatively low velocity injectant mixes with the high-speed flow.

The five-hole probe surveys also yielded the Mach number in the cross stream directions for each case as described earlier. The results are displayed as a grid of vectors each representing a single point showing the direction and relative magnitude of the cross stream Mach number throughout the flow in Figs. 13a–13c. The most notable feature of the flows is the CVP which dominate the flows in the region of the plume. These vortices are formed by the skewed mixing layers on the lateral edges of the jet, see Yuan et al. [28]. Also, in the downstream shock impingement cases in Fig. 13c at the height where the measurement plane crosses above the reflected shock, one can see the change in the vector pattern as the freestream flow angle turns 5.3 deg to become parallel with the wall. Being downstream of the shock reflection caused both the vortex height and spacing to decrease, indicating a decrease in plume size caused by the higher pressure downstream of the shock system. The shock reflecting downstream of the injector causes an additional reduction in the vortex height while only slightly reducing the spacing between the vortices, indicating a reduction in plume penetration but not size.

C. Air Injection Cases

Clearly for unheated air injection into an air stream, concentration surveys are not relevant. Total temperature surveys are also not especially useful, so our efforts were directed at streamwise and transverse Mach number surveys using the five-hole probe.

Streamwise Mach number contour results are given in Fig. 14a–14c, and transverse Mach number component vector plots are given in Fig. 15a–15c. The same qualitative comments made earlier about the corresponding results for methane injection into air apply here also.

A good way to compare these streamwise Mach number results for air or methane injection is to pick a single contour in each case and note its maximum height for comparison. A comparison of this sort is shown in Table 3 below, with the Mach 2.4 contour chosen as representative. Heights are in d_{eff} above the wall. These results seem to indicate that the higher molecular weight air consistently penetrated further than the methane. Comparison with the helium results does not conclusively support or refute this hypothesis.

Two measurements were used to quantitatively characterize the transverse Mach number results. $\mathbb{V}_z$ is the average height of the vortex centers, and $\mathbb{V}_y$ is the horizontal spacing between the vortices, both scaled in terms of d_{eff}. The uncertainty in these measurements is $\pm 0.1 d_{\text{eff}}$. These quantities are tabulated in Table 4.

The vortex dimensions of higher molecular weight air injection were slightly greater, although generally within the margin of error. Comparable data from Maddalena et al.'s studies [13] included only a partial survey of the No-shock case, for which a $\mathbb{V}_z(d_{\text{eff}})$ of approximately 2.0 was estimated. This would seem to indicate significantly lower penetration than found for methane and air injection.

IV. Discussion

A study has been performed on the effects of injectant molecular weight on injection of a transverse jet in three cases: 1) an undisturbed Mach 4 freestream, 2) the same freestream with the addition of a shock wave impinging on the wall 4.5 d_{eff} upstream of the injector center, and 3) with a shock impinging downstream of the injector center between 2–16 d_{eff}. The cases were also compared with one another. The three injectants used were helium injection ($W = 4.00$), methane ($W = 16.04$) and air ($W = 28.97$). The momentum flux ratio and freestream conditions were held constant in all cases. The main results can be summarized as follows. First, higher molecular weight injectant seems to increase penetration, but the effect is weak. It is important to note that even under identical

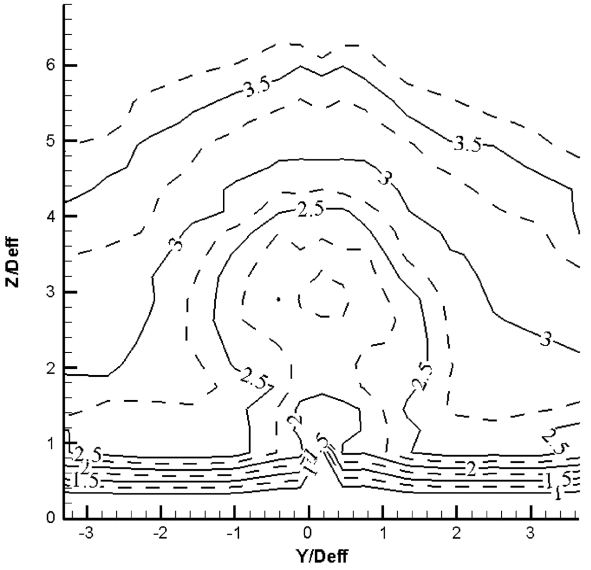

a) Undisturbed flow (No-shock case)

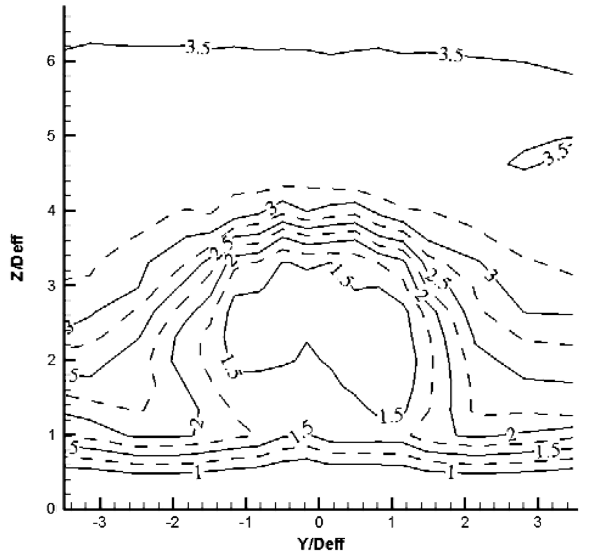

b) Shock impinging downstream of injector at X/d_{eff} = 2.5

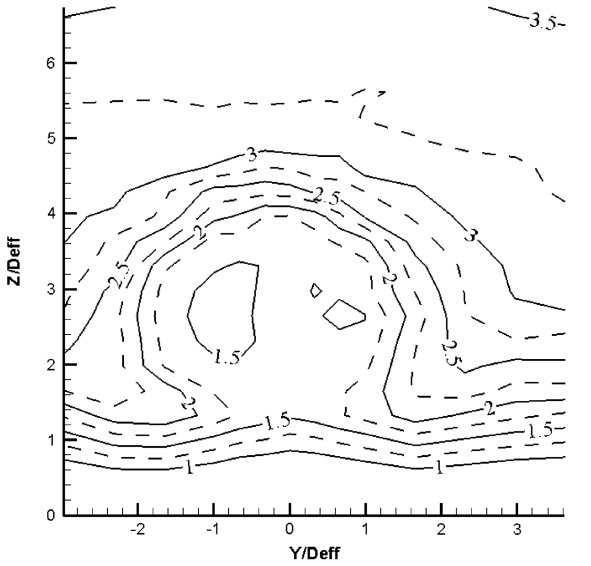

c) Shock impinging upstream of injector at X/d_{eff} = -4.5

Fig. 14 Streamwise Mach number contours in the (*Y*-*Z* plane) at $X/d_{\text{eff}} = 13.9$ for air injection.

jet-to-freestream momentum flux ratio conditions, the jet exit velocity is considerably different for the cases investigated here. Higher molecular weight is accompanied by lower exit velocities, and the development of the large-scale structures present in the jet shear layer is known to depend on the velocity ratio. High molecular weight injectants provide the largest velocity ratio. The dynamics of the jet shear layer is then affected by the injectant molecular weight. Similarly, in their shock-tunnel experiment, Ben-Yakar et al. ([15]), reported that ethylene jet penetrated deeper into the supersonic freestream than hydrogen for the same jet-to-freestream momentum flux ratio. They attributed this result to the evolution of the jet shear layer under large velocity gradients.

Second, the addition of shock waves impinging before, or shortly after the injection jet significantly reduces penetration. Third, the interaction of a shock and an emerging jet increases mixing. When an interface between fluids of differing density is accelerated, the

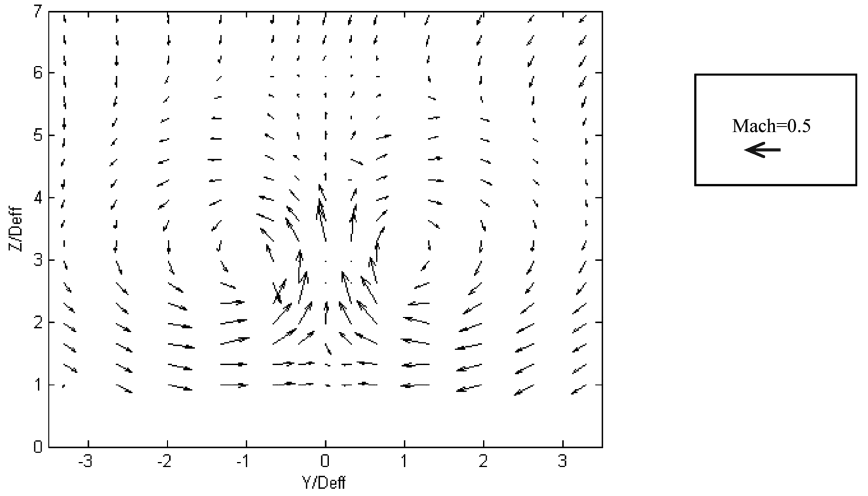

a) Undisturbed flow (No-shock case)

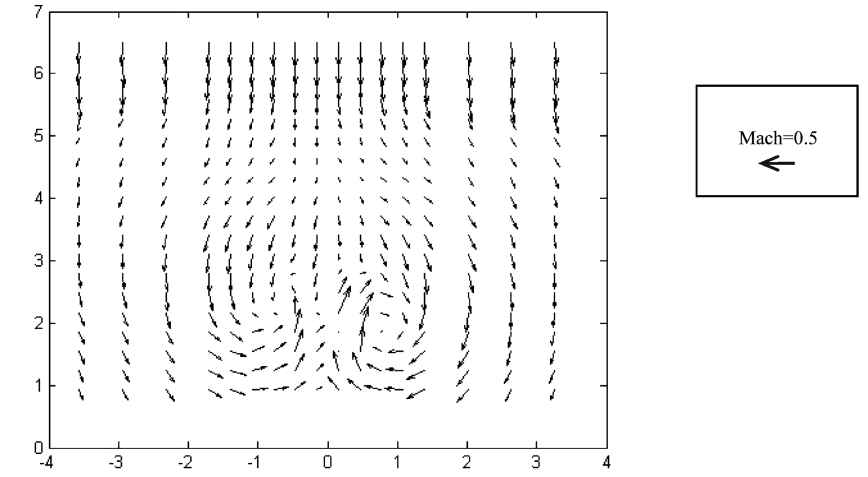

b) Shock impinging downstream of injector at X/d_{eff} = 2.5

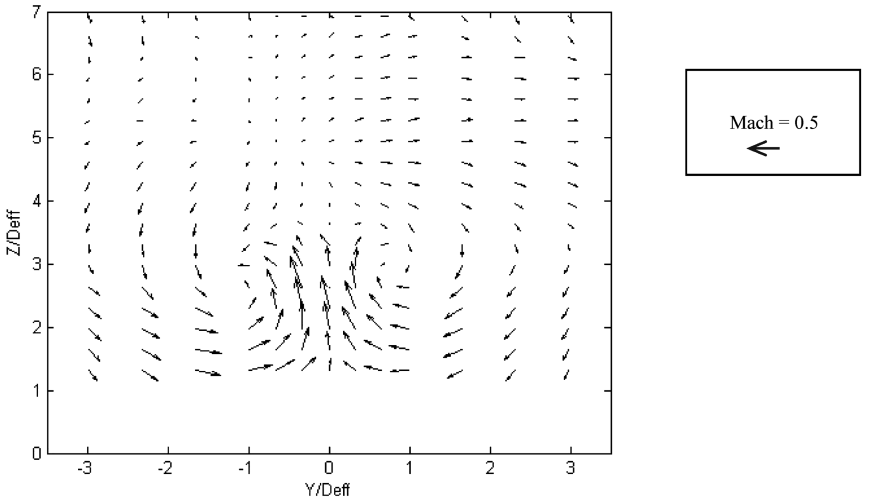

c) Shock impinging upstream of injector at X/d_{eff} = −4.5

Fig. 15 Transverse Mach number contours in the (Y-Z plane) at $X/d_{\mathrm{eff}} = 13.9$ for air injection.

Table 3 Global parameters deduced from Mach number contours

Injectant	Max Mach 2.4 contour height
No shock	
Air	4.0
CH4	3.6
Shock upstream $X/d_{\text{eff}} = -4.5$	
Air	4.3
CH4	4.0
Shock downstream at $X/d_{\text{eff}} = 2.5$	
Air	3.6
CH4	3.3

Table 4 Global parameters of vortices deduced from transverse Mach number data

Injectant	$\mathbb{V}_y(d_{\text{eff}})$	$\mathbb{V}_z(d_{\text{eff}})$
No shock		
Air	2	3.1
CH4	1.9	3
Shock upstream at $X/d_{\text{eff}} = -4.5$		
Air	1.8	2.8
CH4	1.7	2.7
Shock downstream at $X/d_{\text{eff}} = 2.5$		
Air	1.7	2.1
CH4	1.6	2

misalignment of the pressure and density gradients gives rise to instability of the interface and eventually produces turbulent mixing of the fluids. This phenomenon is called the Rayleigh–Taylor instability if the acceleration is sustained and the Richtmyer–Meshkov instability if the acceleration is driven by a shock. Marble et al. [29] first observed that a two-dimensional, unsteady flow was a good analogy for three-dimensional, steady flow produced when an oblique shock impinges on a light gas jet immersed in a coflowing, supersonic air stream. Consider a cylindrical mass of low density gas embedded in a higher molecular weight gas. The discontinuity between the light and heavy gases produces a radially outward density gradient around the circumference of the cylinder. A shock passage over this structure, which can be considered very fast in comparison with other processes, provides a pressure gradient and deposits a distribution of vorticity over the boundary. The baroclinic term, $(\nabla\rho \times \nabla p)/\rho^2$, will vary along the length of the interface due to the varying included angle between the gradients. The magnitude of vorticity will be greatest where the pressure and density gradients are most misaligned. The dynamics of the vorticity, for this simplified geometry, leads to a roll-up of vortices of opposite sign.

Here, we are now considering a transverse light gas jet accompanied by streamwise vorticity. Jet injection into a high-speed crossflow leads to the development of the well-known CVP. Consider for simplicity of explanation only one side of the jet plume containing only one vortex of the vortex pair, and that vortex core is now an approximately circular region of light gas having a strong initial counterclockwise vorticity, surrounded by a coaxial heavy gas stream. In the absence of this vorticity in the CVP, this core area of the plume would behave like the cylindrical mass of low density gas embedded in a higher molecular weight gas discussed above. The vorticity deposited by an impinging shock in the outer half would develop into a clockwise outer vortex, and the vorticity deposited in the inner half would develop into a counterclockwise inner vortex. However, due to the vector nature of the vorticity (that allows algebraic summation) one can expect that the core's strong initial counterclockwise motion vorticity in a jet plume suppresses the additional vorticity development in the outer half and enhances the additional vorticity development in the inner half. This partitioning of the initial vortex core increases the stretching beyond the case with no shock, which ultimately leads to increased mixing. Consider now the shock/transverse injection interaction in the position very near injection where the developing vortical structure has not yet stabilized into a vortex pair. Again, the shock generates additional vorticity of both positive and negative senses, and it is the preferential coalescence of same-sense vorticity that determines the relative dynamics. The earlier the reflected shock hits the jet vortex pair, the less stable is the original vortex pair and the greater the influence and the magnitude of the additional vorticity due to the shock. As the interface thickness increases downstream of the jet exit due to mixing, the local density gradient decreases and the stretching rate from the interaction decreases. Computational studies in [30] support these observations. The magnitude of these effects clearly depends strongly on the initial density difference between the injected fluid and the main stream air. The studies presented here provide data on this influence by parametric variations in the injectant molecular weight from $W = 4$–29.

Flows of this complexity still present a severe challenge to computational simulations. Computational studies in [30,31] and others have highlighted the necessity of adjustments to turbulence models in Reynolds-averaged Navier–Stokes simulations in order to obtain reasonable predictions of these flowfields.

Lastly, one can expect that the process studied here will be important for ignition of real fuel in hot flows. Changes in mixing will affect the local fuel/air ratio, and the shock will increase the local temperature and pressure.

Acknowledgments

This research was supported by the U.S. Air Force Office of Scientific Research under a Multidisciplinary University Research Initiative lead by Paul Dimotakis at California Institute of Technology and by the Air Force Research Lab. through CRAFT Tech, Inc.

References

[1] Spaid, F. W., Zukoski, E. E., and Rosen, R., "A Study of Secondary Injection of Gases into a Supersonic Flow," California Institute of Technology, Jet Propulsion Lab., TR 32-834, Aug. 1966.

[2] Torrence, M. G., "Effect of Injectant Molecular Weight on Mixing of a Normal Jet in a Mach 4 Airstream," NASA TND-6061, 1971.

[3] McClinton, C. R., "The Effect of Injection Angle on the Interaction Between Sonic Secondary Jets and a Supersonic Freestream," NASA TND-6669, Feb. 1972.

[4] Rogers, R. C., "A Study of the Mixing of Hydrogen Injected Normal to a Supersonic Airstream," NASA TN L-7386, March 1971.

[5] Povinelli, L. A., and Ehlers, R. C., "Swirling Base Injection for Supersonic Combustion Ramjets," *AIAA Journal*, Vol. 10, No. 9, 1972, pp. 1243–1244.
doi:10.2514/3.50359

[6] Hartfield, R. J., Hollo, S. D., and McDaniel, J. C., "Experimental Investigations of a Supersonic Swept Ramp Injector Using Laser Induced Iodine Fluorescence," *Journal of Propulsion and Power*, Vol. 10, No. 1, 1994, pp. 129–135.
doi:10.2514/3.23721

[7] Fuller, E. J., Mays, R. B., Thomas, R. H., and Schetz, J. A., "Mixing Studies of Helium in Air at Mach 6," *AIAA Journal*, Vol. 30, No. 9, 1992, pp. 2234–2243.
doi:10.2514/3.11210

[8] Barber, M., Roe, L., and Schetz, J., "Normal, Sonic Helium Injection Through a Wedge-Shaped Orifice into Supersonic Flow," *Journal of Propulsion and Power*, Vol. 13, No. 2, 1997, pp. 257–263.
doi:10.2514/2.5157

[9] Gruber, M. R., Nejad, A. S., Chen, T. H., and Dutton, J. C., "Mixing and Penetration Studies of Sonic Jets in a Mach 2 Freestream," *Journal of Propulsion and Power*, Vol. 11, No. 2, 1995, pp. 315–323.
doi:10.2514/3.51427

[10] Wood, C. W., and Schetz, J. A., "Effects of Unsteady Shock Impingement on High-Speed Gaseous Mixing," AIAA Paper 91-5091, 1991.

[11] Fuller, R. P., Wu, P. K., Nejad, A. S., and Schetz, J. A., "Comparison of Physical and Aerodynamic Ramps as Fuel Injectors in Supersonic Flow," *Journal of Propulsion and Power*, Vol. 14, No. 2, 1998, pp. 135–145.
doi:10.2514/2.5278

[12] Tomioka, S., Jacobsen, L. S., and Schetz, J. A., "Sonic Injection from

Diamond-Shaped Orifices into a Supersonic Crossflow," *Journal of Propulsion and Power*, Vol. 19, No. 1, 2003, pp. 104–14. doi:10.2514/2.6098

[13] Maddalena, L., Campioli, T. L., and Schetz, J. A., "Experimental and Computational Investigation of Light-Gas Injectors in a Mach 4.0 Crossflow," *Journal of Propulsion and Power*, Vol. 22, No. 5, 2006, pp. 1027–38.

[14] Gruber, M. R., Nejad, A. S., Chen, T. H., and Dutton, J. C., "Compressibility Effects in Supersonic Transverse Injection Flowfields," *Physics of Fluids*, Vol. 9, No. 5, 1997, p. 1448. doi:10.1063/1.869257

[15] Ben-Yakar, A., Mungal, M. G., and Hanson, R. K., "Time Evolution and Mixing Characteristics of Hydrogen and Ethylene Transverse Jets in Supersonic Crossflows," *Physics of Fluids*, Vol. 18, No. 2, 2006, p. 026101. doi:10.1063/1.2139684

[16] Gruber, M. R., Carter, C. D., Montes, D. R., Haubelt, L. C., King, P. I., and Hsu, K.-Y., "Experimental Studies of Pylon-Aided Fuel Injection into a Supersonic Flow," *Journal of Propulsion and Power*, Vol. 24, No. 3, 2008, pp. 460–470. doi:10.2514/1.32231

[17] Tomioka, S., Izumikawa, M., Kouchi, T., Masuya, G., Hirano, K., and Matsuo, A., "Matched Pressure Injections into a Supersonic Crossflow Through Diamond-Shaped Orifices," *Journal of Propulsion and Power*, Vol. 24, No. 3, 2008, pp. 471–478.

[18] Srinivasan, R., and Bowersox, R., "Transverse Injection Through Diamond and Circular Ports into a Mach 5.0 Freestream," *AIAA Journal*, Vol. 46, No. 8, 2008, pp. 1944–1962. doi:10.2514/1.29253

[19] Schetz, J. A., *Injection and Mixing in Turbulent Flow*, AIAA, New York, 1980.

[20] Schetz, J. A., Thomas, R. H., and Billig, F. S., "Mixing of Transverse Jets and Wall Jets in Supersonic Flow," *IUTAM Symposium, Separated Flows and Jets*, edited by V. V. Kozlov, and A. V. Dovgal, Springer–Verlag, Berlin, 1991.

[21] Kutschenreuter, P., "Supersonic Flow Combustors," *Scramjet Propulsion*, edited by E. T. Curran and S. N. B. Murthy, AIAA, New York, 2000.

[22] Seiner, J. M., Dash, S. M., and Kenzakowski, D. C., "Historical Review on Enhanced Mixing in Scramjet Engines," *Journal of Propulsion and Power*, Vol. 17, No. 6, 2001, pp. 1273–1286. doi:10.2514/2.5876

[23] Green, S. I., *Fluid Vortices*, Kluwer, Dordrecht, The Netherlands, 1995.

[24] Ingenito, A., and Bruno, C., "Physics and Regimes of Supersonic Combustion," *AIAA Journal*, Vol. 48, No. 3, 2010, pp. 515–525. doi:10.2514/1.43652

[25] Zubkov, A. I., and Glagolev, A. I., "The Effect of Boundary Layer Thickness and Transverse Curvature of the Surface on the Geometry and Forces Acting in the Separation Zone Produced by Injection of a Jet into Supersonic Flow over that Surface," *Fluid Mechanics: Soviet Research*, Vol. 8, No. 1, 1979, pp. 69–79.

[26] W. F. Ng., F. T. Kwok, and T. A. Ninnemann, "A Concentration Probe for the Study of Mixing in Supersonic Shear Flows," AIAA Paper 89-2459, July 1989.

[27] Centolanzi, F. J., "Characteristics of a 40 Degree Cone for Measuring Mach Number, Total Pressure, and Flow Angles at Supersonic Speed," NACA TN-3967, May 1957.

[28] Yuan, L. L., Street, R. L., and Ferziger, J. H., "Large Eddy Simulation of a Round Jet in Crossflow," *Journal of Fluid Mechanics*, Vol. 379, Jan. 1999, pp. 71–104. doi:10.1017/S0022112098003346

[29] Marble, F. E., Zukoski, J. W., Jacobs, J. W., Hendricks, G. J., and Waitz, I. A., "Shock Enhancement and Control of Hypersonic Mixing and Combustion," AIAA Paper 90-1981, 1981.

[30] Campioli, T. L., "Computational Studies of Penetration and Mixing for Complex Jet Injectors to Aid in Design of Hypersonic Systems," Ph.D. Dissertation, Virginia Polytechnic Institute and State University, Blacksburg, VA, June 2007.

[31] Burger, S. K., Schetz, J. A., and Ungewitter, R., "Effects of Injectant Molecular Weight on Transverse Injection Mixing Processes in Supersonic Flow," AIAA Paper 2009-7315, 2009.

R. Bowersox
Associate Editor